

Dynamic Chunking Diffusion Transformer

Akash Haridas^{*1} ✨ Utkarsh Saxena¹ Parsa Ashrafi Fashi¹
 Mehdi Rezagholizadeh¹ ✨ Vikram Appia¹ Emad Barsoum¹
¹Advanced Micro Devices Inc. (AMD)

✨ Correspondence to: akash.haridas@amd.com, mehdi.rezagholizadeh@amd.com.

Abstract

Diffusion Transformers process images as fixed-length sequences of tokens produced by a static *patchify* operation. While effective, this design spends uniform compute on low- and high-information regions alike, ignoring that images contain regions of varying detail and that the denoising process progresses from coarse structure at early timesteps to fine detail at late timesteps. We introduce the *Dynamic Chunking Diffusion Transformer* (DC-DiT), which augments the DiT backbone with a learned encoder-router-decoder scaffold that adaptively compresses the 2D input into a shorter token sequence in a data-dependent manner using a chunking mechanism learned end-to-end with diffusion training. The mechanism learns to compress uniform background regions into fewer tokens and detail-rich regions into more tokens, with meaningful visual segmentations emerging without explicit supervision. Furthermore, it also learns to adapt its compression across diffusion timesteps, using fewer tokens at noisy stages and more tokens as fine details emerge. On class-conditional ImageNet 256×256 , DC-DiT consistently improves FID and Inception Score over both parameter-matched and FLOP-matched DiT baselines across $4\times$ and $16\times$ compression, showing this is a promising technique with potential further applications to pixel-space, video and 3D generation. Beyond accuracy, DC-DiT is practical: it can be upcycled from pretrained DiT checkpoints with minimal post-training compute (up to $8\times$ fewer training steps) and composes with other dynamic computation methods to further reduce generation FLOPs.

1 Introduction

Transformer-based diffusion models achieve strong image generation quality, but existing architectures commonly rely on fixed tokenization schemes that result in equal amounts of compute being spent across spatial regions and diffusion timesteps. Common Diffusion Transformer (DiT) [1] based models apply a *patchify* operation to transform a 2D input into a token sequence: fixed-size non-overlapping patches of the 2D input are flattened into tokens, resulting in both low- and high-information spatial regions being represented by the same number of tokens. Furthermore, an identical *patchify* operation is applied at every diffusion timestep. This ignores two sources of natural adaptivity in image diffusion: different image spatial regions contain different amounts of detail, and diffusion trajectories typically progress from coarse structure at early timesteps to fine details at late timesteps.

In the language modelling domain, recent works have explored foregoing the pre-trained tokenizers commonly used to convert text strings into token sequences and instead training directly on the UTF-8 encoded bytes of the text. Such approaches merge bytes into tokens in a dynamic and data-dependent manner either through rule-based heuristics [2, 3] or through end-to-end learned byte-level or token-level chunking mechanisms [4, 5]. Such methods have been shown to learn meaningful token boundaries without explicit supervision and improve model scaling and efficiency.

To address the natural adaptivity in image diffusion, we propose the Dynamic Chunking Diffusion Transformer (DC-DiT). We adapt the end-to-end learned dynamic chunking mechanism from H-Net [4] originally designed for causal sequence modeling and modify it for non-causal spatial processing. The core insight is that spatially nearby tokens with high similarity can be merged into a single token for processing. We show that the chunking mechanism learns meaningful

visual segmentations during end-to-end diffusion training without any explicit supervision: background regions with low variation are compressed into fewer tokens and object regions with high variation are represented by more tokens. Furthermore, the mechanism naturally learns to compress noisier timesteps into fewer tokens and use more tokens as the image becomes cleaner, following the coarse-to-fine refinement of the diffusion process. We also show that by learning to re-allocate compute across spatial regions and timesteps, DC-DiT achieves better FID and Inception Scores compared to both parameter-matched and FLOP-matched standard DiT baselines across compression ratios from $4\times$ to $16\times$, with advantages that are pronounced at higher compression ratios where differentiating between informative and redundant regions becomes more important.

Contributions. Our contributions can be summarized as follows:

- We propose DC-DiT, a Diffusion Transformer that learns to adaptively compress the 2D input into a token sequence in a data-dependent manner with a mechanism learned end-to-end during diffusion training.
- We adapt H-Net-style dynamic chunking mechanism for spatial processing and show that it naturally learns meaningful visual segmentations and timestep-wise compression schedules during end-to-end diffusion training without any explicit supervision.
- We show that by learning to re-allocate compute across spatial regions and timesteps, DC-DiT achieves better FID and Inception Scores compared to both parameter-matched and FLOP-matched standard DiT that uses fixed patchification.
- We demonstrate *upcycling* a pre-trained DiT that uses fixed patchification into a DC-DiT that uses dynamic chunking with minimal post-training compute, achieving better results than training from scratch.

2 Related Work

Compute-adaptive Diffusion Transformers. DiT [1] applies uniform computation at every spatial position and denoising step. A growing body of work adapts compute along spatial and temporal axes: DyDiT [6] adjusts hidden dimension per timestep and prunes uninformative spatial tokens; D²iT [7] encodes regions at different downsampling rates via a Dynamic VAE. Token-level routing methods include DiffCR [8], which learns per-layer compression ratios, SparseDiT [9], which varies token density by layer depth, and DiffMoE [10], which integrates mixture-of-experts with dynamic capacity allocation. Inference-time approaches such as importance-based token merging [11] and GRAT [12] avoid retraining altogether.

Adaptive visual tokenization. Outside diffusion, content-adaptive tokenization has been studied in vision and vision-language models. DynamicViT [13] progressively prunes tokens via learned importance scores, while APT [14] allocates variable-size patches based on local information content. Variable-length encoders such as ALIT [15], ElasticTok [16], and DOVE [17] emit token counts conditioned on image content.

Learned boundaries in language modeling. A key motivation for DC-DiT comes from recent language modeling work that replaces fixed tokenization with dynamic, data-dependent merging. BLT [2] operates directly on raw bytes and segments them into variable-length patches using entropy-based heuristics, reallocating computation toward high-information transitions. SuperBPE [3] learns cross-whitespace merges that reduce sequence length at inference time. Moving beyond rule-based segmentation, H-Net [4] introduces end-to-end trainable dynamic chunking: it predicts boundary tokens from local similarity, routes computation through a compressed sequence, and reconstructs the full output via a learned de-chunking operator, discovering meaningful segment boundaries without explicit supervision. DLCM [5] extends this idea by learning semantic boundaries from latent representations and shifting computation from tokens to a compressed concept space. Collectively, these methods demonstrate that variable-length abstractions shift computation toward high-information regions of a sequence. DC-DiT adapts this principle to the visual domain: we adopt H-Net’s encoder-router-decoder scaffold and specialize it for 2D spatial tokens and diffusion conditioning.

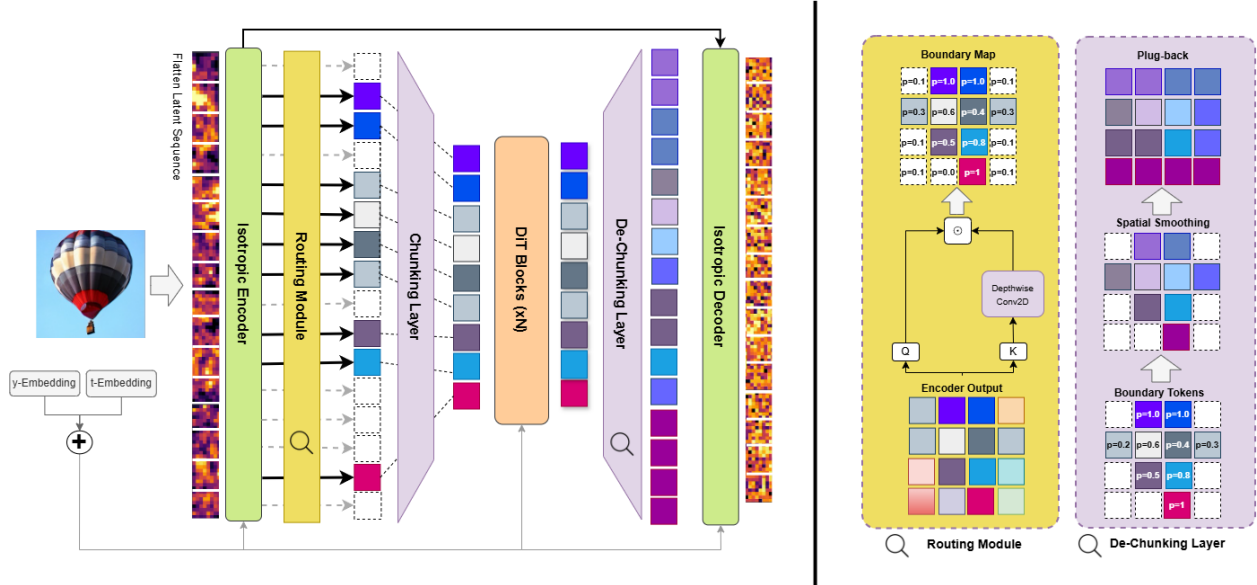


Figure 1: Architecture of DC-DiT. The isotropic encoder aggregates local context across the input tokens. The chunking layer selects a subset of boundary tokens via a learned routing module, yielding a compressed sequence that is processed by the DiT blocks. The de-chunking layer restores the original resolution through spatial smoothing followed by plug-back.

3 Method

Unlike the fixed patching mechanism of DiT, DC-DiT learns to perform data-dependent dynamic chunking of the 2D input into vision tokens jointly with diffusion training. We adopt architectural components from H-Net [4], originally designed for causal language modeling, and modify it for non-causal spatial processing. Compared to a traditional DiT, DC-DiT additionally consists of an encoder, a chunking (router) layer, a de-chunking layer, and a decoder.

3.1 Overall architecture

The standard DiT applies a fixed patching operation to the input latent image by grouping together non-overlapping $P \times P$ patches, where $P > 1$ is a hyperparameter fixed during both training and inference [1], resulting in a P^2 compression ratio. In contrast, DC-DiT applies a patchify operation with $P = 1$, which effectively just flattens the latent image into a token sequence. The grouping of nearby latent pixels into combined vision tokens is performed by a dynamic and data-dependent chunking mechanism learned end-to-end jointly with the diffusion model.

The flattened token sequence passes through an isotropic encoder whose main purpose is to aggregate multiple neighboring tokens into consolidated representations, which allows the subsequent chunking layer to dynamically decide which tokens to drop and which to keep. Intuitively, the chunking layer *drops* tokens whose consolidated representations are similar enough to that of neighboring tokens and *keeps* tokens that sufficiently represent its neighboring dropped tokens. Therefore, the role of the encoder is to mix information between tokens to enable such a dynamic chunking mechanism.

This compressed token sequence is processed by DiT blocks. For controlled experiments, we keep the design of the DiT blocks the same as [1], with adaLN-Zero layers for conditioning. After the DiT blocks, the de-chunking layer decompresses the sequence back to its original resolution. The isotropic decoder finally maps the tokens sequence back to the prediction space of the diffusion model. A residual connection from the encoder output is added after de-chunking and before the decoder, carrying fine-grained spatial information around the compressed inner network. The residual is gated by the router’s boundary probabilities via a straight-through estimator (STE) [18], which preserves the discrete

routing decisions in the forward pass while allowing gradients to propagate through the routing probabilities during training.

Therefore at a high level, DC-DiT comprises of an encoder-router-decoder scaffold around a denoising network that operates on a shortened sequence:

1. An **encoder** mixes information across the token sequence, lifting the features into a representation suitable for routing.
2. A **chunking layer** consisting of a routing module predicts which tokens are *boundaries* (kept) vs. *non-boundaries* (dropped), inducing a shorter sequence.
3. An inner **main network** consisting of DiT blocks operates on the shortened sequence. Sinusoidal positional embeddings are added to the token sequence immediately before this network, indexed by each retained token’s original 2D grid position.
4. A **de-chunking layer** reconstructs the original resolution token sequence.
5. A **decoder** maps the tokens sequence back to the prediction space of the diffusion model.

3.2 Encoder and Decoder

The encoder and decoder are isotropic blocks that preserve token count while mixing information across the 2D spatial grid. The encoder’s role is to aggregate local context so that the subsequent router can make informed boundary decisions, and the decoder maps the features after de-chunking back to the prediction space of the diffusion model.

For the isotropic block architecture, we use convolutional residual blocks following [19]. Each block reshapes the token sequence to a 2D feature map of shape (H, W, D) , then applies two 3×3 2D convolutions interleaved with GroupNorm and SiLU activations. The conditioning vector is added after the first convolution, and a residual connection is applied after the second convolution. The output is flattened back to a token sequence.

Since the encoder and decoder operate on the uncompressed input, computational efficiency is an important consideration. Therefore, they operate at an intermediate hidden dimension one-quarter of the main transformer dimension, projecting up to the full dimension only at the encoder output (where routing operates) and back down at the decoder input.

We also experimented with Mamba-style SSM mixers and attention-based blocks but chose to use the convolutional blocks for its relative simplicity and cleaner visual segmentations produced by the following chunking layer.

3.3 Chunking Layer

The chunking layer converts a full sequence $X \in \mathbb{R}^{B \times L \times d}$ into a shorter sequence $X' \in \mathbb{R}^{B \times M \times d}$ by selecting a subset of tokens as *boundary tokens*. The selection is produced by a lightweight routing module.

Routing score and boundary probability. The router maps token features to a boundary probability $p_i \in [0, 1]$ and a hard boundary mask. H-Net [4] computes boundaries in **causal sequential** (1D) fashion: it projects tokens to query and key vectors, computes the cosine similarity $s_i \in [-1, 1]$ between adjacent token pairs, and converts similarity to a boundary probability via $p_i = (1 - s_i)/2$. Intuitively, high cosine similarity between neighbors yields a low boundary probability (the tokens belong to the same segment), while low similarity signals a semantic transition and produces a high boundary probability.

We adapt this mechanism for **spatial** (2D) processing. We project token features into separate query and key vectors via learned linear projections W_Q and W_K (both initialized to the identity), then ℓ_2 -normalize and reshape them to an $(H \times W)$ grid. To efficiently aggregate neighbor key vectors, we apply a depthwise 3×3 convolution initialized as a uniform averaging kernel, producing a normalized average of neighboring key vectors $\bar{\mathbf{k}}_i$ in a single pass. The similarity score for each token is then the dot product $s_i = \mathbf{q}_i \cdot \bar{\mathbf{k}}_i$, which approximates the average cosine similarity of the token’s query to its spatial neighbors’ keys. This is converted to a boundary probability via the same formula as H-Net: $p_i = (1 - s_i)/2$. Tokens whose query is dissimilar to the local key context receive high boundary probability

and are retained, while tokens whose query aligns with the surrounding key average are candidates for dropping. We obtain a hard boundary mask by thresholding at $p > 0.5$.

Batched chunking and padding. During batched training, each sample may have a different number of boundary tokens M selected by the router. To facilitate batched training, we pad the batch after chunking upto the maximum number of boundary tokens M_{\max} in the batch. The padding slots, often small in number, are filled with the next highest-probability non-boundary tokens. This yields a simple implementation of batched training.

3.4 De-chunking Layer

After the inner network processes the shortened sequence, we reconstruct the token sequence back to its original resolution via a de-chunking operator. De-chunking has two conceptual components: **smoothing** over boundary-token representations and a **plug-back** map that assigns each original token position a boundary-derived representation.

Motivation for smoothing. Because chunking involves hard discrete decisions (each token is either kept or dropped), the boundary between two chunks can shift by a single position due to a small change in the router’s output. Without smoothing, such a shift would abruptly reassign all downstream tokens to a different boundary representation, creating a discontinuity that is difficult to optimize through. H-Net [4] addresses this in the causal 1D case with an EMA scan whose decay rate is the boundary probability: at confident boundaries ($p \approx 1$) the representation resets to the boundary’s own features, while at uncertain boundaries ($p \approx 0$) it carries forward from the previous token, attenuating the effect of uncertain decisions and making the de-chunking differentiable. We adapt this idea to the 2D spatial setting with a confidence-weighted Gaussian kernel, described below.

Spatial smoothing. We blend boundary-token representations using a spatial Gaussian kernel. Let $\mathbf{h}_i \in \mathbb{R}^D$ denote the representation of boundary token i at 2D grid position (r_i, c_i) with boundary probability p_i . We first compute pairwise squared Euclidean distances $d_{ij}^2 = (r_i - r_j)^2 + (c_i - c_j)^2$ and apply a Gaussian kernel weighted by the source token’s confidence:

$$W_{ij} = \exp\left(-\frac{d_{ij}^2}{2\sigma^2}\right) \cdot p_j, \quad \tilde{W}_{ij} = \frac{W_{ij}}{\sum_k W_{ik}}.$$

At each boundary token, a smoothed representation of all other boundary tokens $\tilde{\mathbf{h}}_i = \sum_j \tilde{W}_{ij} \mathbf{h}_j$ is computed and blended with its original representation based on its own confidence:

$$\mathbf{h}_i^{\text{out}} = p_i \mathbf{h}_i + (1 - p_i) \tilde{\mathbf{h}}_i.$$

High-confidence boundaries retain their original features, while low-confidence boundaries are smoothed toward their spatial neighbors. This mirrors the role of H-Net’s EMA decay and generalizes naturally to 2D by replacing the sequential carry-forward with a distance-weighted spatial blend.

The **plug-back** map then reconstructs the full L -token grid by assigning each original grid position the representation of its spatially nearest boundary (Euclidean distance on the 2D grid).

3.5 Training objective

We train DC-DiT with the same diffusion training objective as in DiT [1]. In addition, we include a lightweight regularizer following the load balancing mechanism of Mixture-of-Experts models [20] that encourages a target average downsampling factor $N > 1$ for the routing module. Concretely, for a routing module output with boundary mask $m \in \{0, 1\}^{B \times L}$ and boundary probabilities $p \in [0, 1]^{B \times L}$, we define $\hat{r} = \mathbb{E}[m]$ and $\bar{p} = \mathbb{E}[p]$. We use the following regularizer:

$$\mathcal{L}_{ratio} = \frac{N}{N - 1} ((1 - \hat{r})(1 - \bar{p}) + (N - 1)\hat{r}\bar{p}).$$

The overall loss is $\mathcal{L} = \mathcal{L}_{diffusion} + \lambda\mathcal{L}_{ratio}$, where λ is a tunable weight. The ratio loss steers the router toward a target average compression ratio but does not enforce it exactly; the model converges to a ratio near, but not equal to, N , as also observed in H-Net [4].

4 Experiments and Results

We evaluate DC-DiT on class-conditional image generation on ImageNet 256×256 and compare against DiT baselines that use fixed patchification under both parameter-matched and FLOP-matched conditions.

4.1 Experimental setup

We evaluate on class-conditional ImageNet 256×256 generation and report FID-50K and Inception Score (IS) as our primary generation quality metrics. We use the same diffusion formulation as standard DiT [1]: a linear noise schedule with 1000 diffusion steps during training, and DDPM sampling with 250 steps during evaluation. All models operate in the latent space of a pretrained Stable Diffusion VAE encoder [19], with class conditioning via adaLN-Zero.

Model configurations. We train two DC-DiT variants at different model scales:

- **DC-DiT-B** (138M parameters): Uses the DiT-B transformer backbone (12 blocks, hidden dimension 768, 12 attention heads) as the inner denoising network, augmented with the encoder-router-decoder scaffold. The encoder and decoder each consist of two convolutional residual blocks operating at an intermediate hidden dimension of 192 (1/4th of the transformer dimension).
- **DC-DiT-XL** (690M parameters): Uses the DiT-XL transformer backbone (28 blocks, hidden dimension 1152, 16 attention heads) as the inner denoising network, with the same encoder-router-decoder design using two convolutional residual blocks each operating at an intermediate hidden dimension of 288.

Each variant is trained at two target compression ratios: $N=4$ and $N=16$, set via the ratio loss \mathcal{L}_{ratio} . The $N=4$ setting targets moderate compression comparable to patch size $P=2$ in standard DiT, while $N=16$ targets aggressive compression comparable to $P=4$. As reported in the Avg CR column of Table 1, the achieved compression ratios are close to but not exactly equal to the target N , consistent with the soft nature of the ratio loss.

Baselines. For each DC-DiT variant and compression setting, we construct two DiT baselines that use fixed patchification:

- **Isoparam** (parameter-matched): A standard DiT with approximately the same parameter count as the corresponding DC-DiT.
- **Isoflop** (FLOP-matched): A standard DiT augmented with additional transformer layers to approximately match the per-image inference FLOPs of the corresponding DC-DiT.

Since the DC-DiT’s encoder and decoder blocks operate on the uncompressed input, they incur greater FLOPs overhead relative to their modest parameter count. Therefore, under the isoflop setting, DC-DiT has significantly fewer parameters than the corresponding DiT baseline.

Training All models are trained for 400K steps with a global batch size of 256 using the AdamW optimizer with a learning rate of 1×10^{-4} . For DC-DiT, the ratio loss weight is set to $\lambda=0.03$ after performing a grid search. All models were trained on AMD Instinct MI325X and MI300X GPUs.

Table 1: Class-conditional ImageNet 256×256 generation results at 400K training steps. DC-DiT outperforms both parameter-matched (isoparam) and FLOP-matched (isoflop) DiT baselines across model scales and compression ratios. Best values per group are **bolded**.

Model	# Params	TFLOPs/img	Avg CR	FID ↓	IS ↑	Prec ↑	Rec ↑
<i>B-scale, $\sim 4 \times$ compression</i>							
DiT, $P=2$, isoparam	141M	24.84	4.0	19.45	73.95	0.65	0.56
DiT, $P=2$, isoflop	180M	32.50	4.0	15.78	86.50	0.69	0.54
DC-DiT, $N=4$ (ours)	138M	32.72	4.49	13.51	96.30	0.72	0.55
<i>B-scale, $\sim 16 \times$ compression</i>							
DiT, $P=4$, isoparam	141M	6.01	16.0	44.31	36.01	0.46	0.54
DiT, $P=4$, isoflop	301M	12.92	16.0	30.82	51.49	0.55	0.55
DC-DiT, $N=16$ (ours)	138M	12.98	17.2	29.92	61.84	0.57	0.53
<i>XL-scale, $\sim 4 \times$ compression</i>							
DiT, $P=2$, isoparam	699M	122.41	4.0	13.14	99.91	0.69	0.55
DiT, $P=2$, isoflop	818M	143.75	4.0	7.82	132.59	0.75	0.55
DC-DiT, $N=4$ (ours)	690M	147.50	4.4	7.17	140.90	0.79	0.53
<i>XL-scale, $\sim 16 \times$ compression</i>							
DiT, $P=4$, isoparam	699M	29.96	16.0	20.01	73.84	0.64	0.55
DiT, $P=4$, isoflop	1201M	51.65	16.0	16.35	86.74	0.67	0.54
DC-DiT, $N=16$ (ours)	690M	50.89	15.61	13.60	110.93	0.70	0.53

4.2 Main Results

Table 1 compares DC-DiT with DiT baselines after 400K training steps. DC-DiT consistently achieves significantly better scores than parameter-matched baselines across model scales and compression ratios. Compared to the stronger FLOP-matched baselines, DC-DiT still achieves improvements across all settings despite having significantly fewer parameters, in some cases less than half of the baseline (301M vs. 138M at B-scale $16 \times$). These results demonstrate the consistent benefit of dynamic chunking over fixed patchification by re-allocating the compute budget towards more informative spatial regions and timesteps.

Figure 3 shows that DC-DiT achieves similar FID as the isoparam baselines with 25-50% fewer training steps. At XL scale with $\sim 4 \times$ compression, DC-DiT initially lags both baselines while the router learns meaningful boundary probabilities, but converges more steeply and overtakes both by 400K steps.

Learned spatial segmentation. Figure 2 visualizes the router’s boundary predictions on representative ImageNet samples. The router assigns high boundary probability to tokens corresponding to object edges, fine textures, and regions of high local variation, while tokens corresponding to uniform backgrounds and low-variation areas are classified as non-boundaries and dropped from the inner sequence. This behavior emerges purely from the diffusion training objective without any explicit supervision for segmentation or boundary detection. The result is an implicit content-adaptive tokenization in which background regions with low variation are compressed into fewer tokens and object regions with high variation are represented by more tokens.

Timestep-adaptive compression. Beyond spatial adaptivity, DC-DiT’s chunking mechanism also adapts its compression across the diffusion trajectory. Figure 4 plots the learned compression ratio and the resulting inference throughput as a function of diffusion timestep for set of generated samples. At early timesteps, when the input is dominated by noise and contains little recoverable spatial structure, the router aggressively compresses the sequence, retaining fewer boundary tokens and yielding higher throughput. As denoising progresses and the image transitions from coarse structure to fine detail, the router progressively retains more tokens, allocating additional compute to the later timesteps. This behavior follows the coarse-to-fine refinement inherent to the diffusion process: noisy timesteps process global structure, while clean timesteps process fine-grained detail. The compression schedule is not prescribed by any explicit

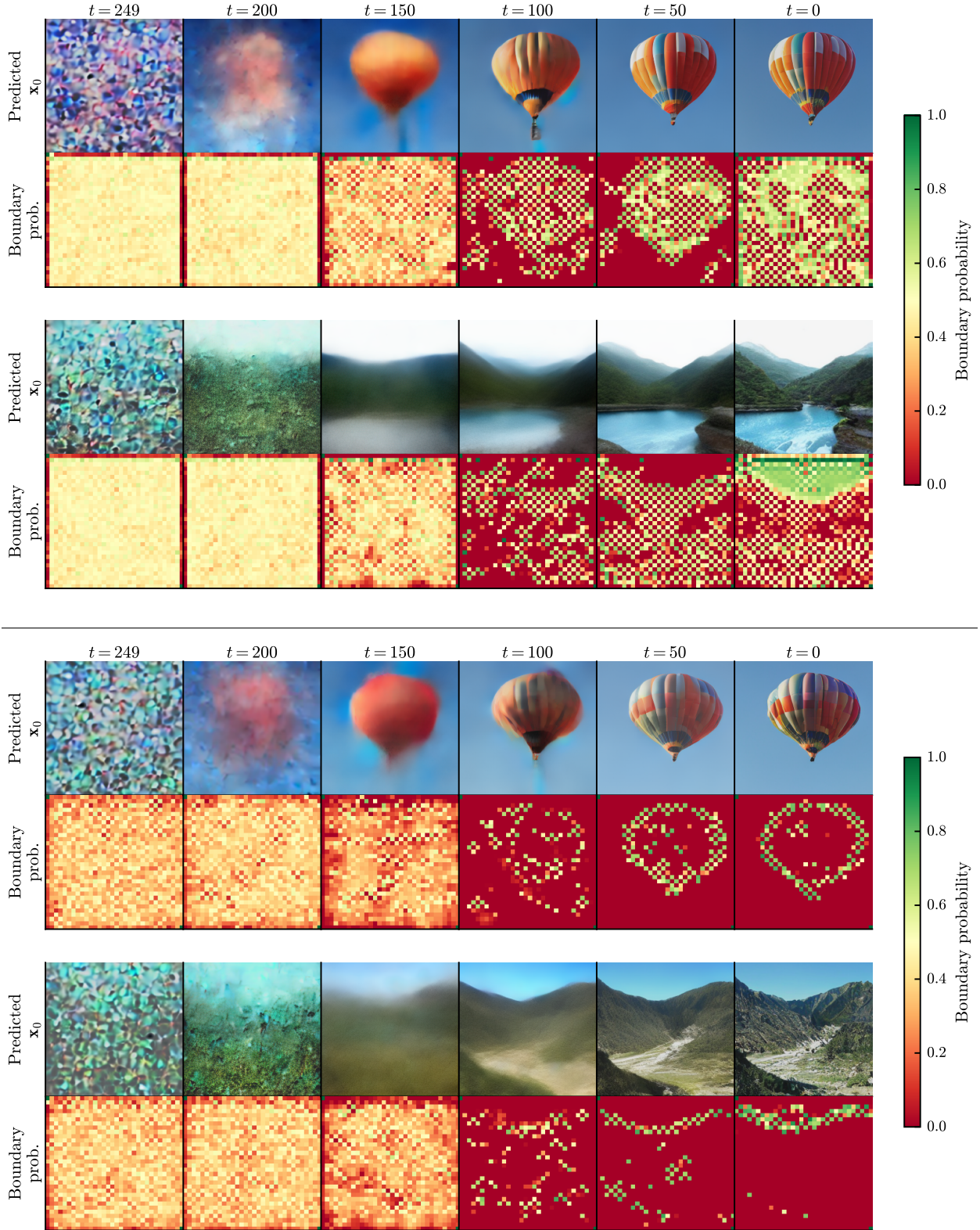


Figure 2: Boundary predictions shown next to sample images from the XL-scale DC-DiT at $N=4$ (top) and $N=16$ (bottom). Boundary tokens (retained) concentrate on object edges and textured regions, while non-boundary tokens (dropped) cluster in uniform backgrounds. The chunking mechanism discovers these visual segmentations without any explicit supervision, solely from being trained with the diffusion objective.

timestep-dependent heuristic: it emerges from the diffusion training objective, as the router learns that different timesteps benefit from different token budgets.

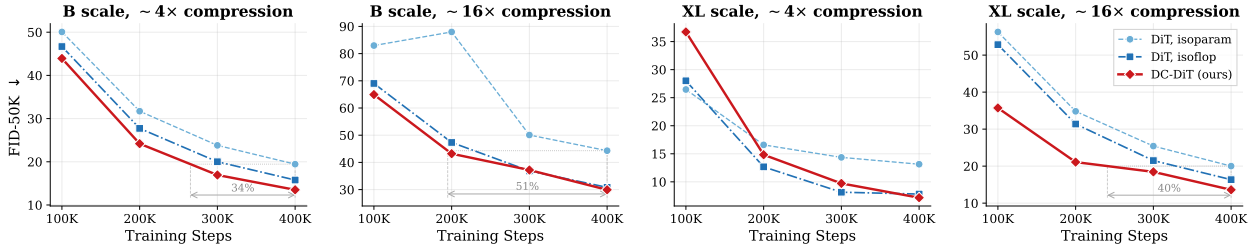


Figure 3: FID-50K as a function of training steps across model scales and compression ratios. DC-DiT achieves similar scores as the isoparam baselines with 25-50% fewer training steps. At XL scale with $\sim 4\times$ compression, DC-DiT starts with higher FID but exhibits faster convergence, surpassing both baselines by 400K steps.

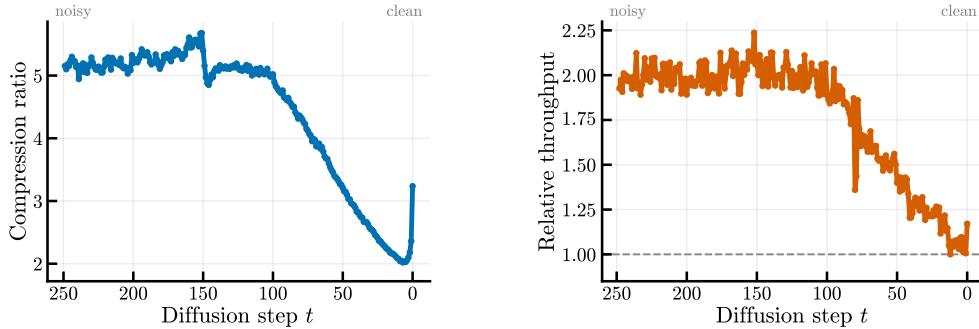


Figure 4: Compression ratio and inference throughput as a function of diffusion timestep for the XL-scale DC-DiT. At early (noisy) timesteps the router retains fewer boundary tokens, yielding higher compression and faster throughput. As denoising progresses and fine details emerge, the router retains more tokens. This schedule emerges entirely from end-to-end training without any explicit timestep-dependent supervision.

4.3 Ablation with random boundary selection

The encoder-router-decoder scaffold compresses the sequence regardless of how boundary tokens are chosen. To isolate the contribution of the router’s learned predictions, we train a variant that selects boundaries uniformly at random, keeping all other components identical. Table 2 shows that FID and Inception Score both worsen under random selection (B-scale, $N=4$), confirming that content-adaptive boundary token selection (retaining tokens in high-information regions) is a meaningful contribution.

Table 2: Ablation of learned vs. random boundary selection on ImageNet 256×256 , B-scale, $N=4$ (400K steps). Random boundaries replace the router with uniform random selection; all other components are identical. Best values are **bolded**.

Model	FID ↓	IS ↑
DiT, $P=2$, isoflop	15.78	86.50
DC-DiT, $N=4$, random boundaries	16.69	91.00
DC-DiT, $N=4$ (ours)	13.51	96.30

Table 3: Upcycling results for the XL-scale DC-DiT on ImageNet 256×256 . “From scratch” denotes DC-DiT training from random initialization (400K steps). “Upcycled” initializes the inner DiT blocks from the official pretrained DiT-XL/2 checkpoint [1], originally trained for 7M steps ($17.5 \times$ our 400K budget), with frozen embedders and a conditioning adaptor. “+ Distilled” adds a 5K-step activation-distillation warm-up similar to by [21]. Best results are **bolded**.

Model	Method	Steps	%	FID ↓	IS ↑	Prec ↑	Rec ↑
DiT, $P=2$	Baseline	400K	100	7.82	132.59	0.75	0.55
DC-DiT	From scratch	400K	100	7.17	140.90	0.79	0.53
DC-DiT	Upcycled	20K	5	184.74	3.86	0.05	0.00
DC-DiT	Upcycled	50K	12.5	14.55	127.33	0.63	0.62
DC-DiT	Upcycled	100K	25	6.48	181.22	0.71	0.61
DC-DiT	Upcycled + Distilled	20K	5	11.01	150.41	0.66	0.59
DC-DiT	Upcycled + Distilled	50K	12.5	4.97	199.70	0.73	0.63
DC-DiT	Upcycled + Distilled	100K	25	5.43	201.68	0.71	0.62

4.4 Upcycling from pretrained DiT

DC-DiT wraps a standard DiT backbone inside the encoder-router-decoder scaffold. Therefore, the inner DiT blocks can be initialized from a pretrained DiT checkpoint and converted to use dynamic chunking with a small compute budget, a process we refer to as *upcycling*. This is particularly attractive because high-quality pretrained DiT-like checkpoints are publicly available and training large diffusion models from scratch is expensive; upcycling amortizes this cost by reusing the backbone’s learned representations and training only the lightweight encoder-router-decoder modules. We found that naive upcycling causes the timestep and class embedders to drift during training, destabilizing the conditioning vector that the pretrained adaLN-Zero layers rely on. We found that freezing the pretrained timestep and class embedders and applying a trainable LayerNorm adaptor on the condition vector inside the encoder and decoder modules effective at stabilizing upcycling. To further accelerate convergence we add a short *activation distillation* warm-up phase, similar to the grafting approach of [21] which demonstrated that block-level distillation from a teacher model significantly accelerates architectural adaptation of DiTs. Concretely, a frozen copy of the pretrained DiT serves as the teacher, and the full DC-DiT student is trained for a brief warm-up (5K steps) with an MSE loss between student and teacher block outputs, aligning the new encoder-decoder modules with the pretrained backbone before switching to the standard diffusion objective.

Table 3 summarizes the upcycling results for the XL-scale DC-DiT alongside the standard DiT-XL baseline. The pretrained DiT-XL/2 backbone is the official release from [1], trained for 7M steps on the same ImageNet 256×256 dataset: $17.5 \times$ our 400K training budget. With activation distillation, upcycling is highly effective: at only 12.5% of the training budget, the distilled model already surpasses both the from-scratch DC-DiT and the DiT baseline trained for the full 400K steps. Even without distillation, upcycling at 25% of the budget outperforms both full-budget baselines. Activation distillation is critical for early convergence: at just 5% of the budget, the distilled model already produces competitive generation quality, whereas the non-distilled model has barely begun to converge at the same point. This confirms that the short distillation warm-up is essential for bridging the distribution gap between the pretrained backbone and the new encoder-decoder modules.

4.5 Composability with other dynamic computation techniques

While DC-DiT introduces data-dependent dynamic patchification to improve the diffusion process, several recent works focus on dynamic execution strategies to reduce computational FLOPs during generation [6, 7, 8]. Among these, the seminal work DyDiT [6] dynamically adjusts computation along both the timestep and spatial dimensions during generation. Specifically, DyDiT proposes a timestep-wise dynamic width mechanism, which adapts the model width conditioned on the generation timestep, and a spatial-wise dynamic token strategy that avoids redundant computation at spatial locations deemed unnecessary. Conceptually, DC-DiT and DyDiT address different aspects of efficiency. DC-DiT introduces content-adaptive patchification, whereas DyDiT focuses on dynamic computation within the DiT backbone to reduce compute cost. In principle, these two approaches are orthogonal and therefore compatible with

Table 4: Class-conditional ImageNet 256×256 generation results at 400K training steps. DC-DiT outperforms both parameter-matched (isoparam) and FLOP-matched (isoflop) DiT baselines across model scales and compression ratios. Best values per group are **bolded**.

Model	TFLOPs/img	FID ↓	IS ↑	Prec ↑	Rec ↑
<i>B-scale, $\sim 4 \times$ compression</i>					
DyDiT $_{\lambda=0.7}$, $P=2$, isoflop	22.75	15.47	90.40	0.67	0.57
DC-DiT + DyDiT $_{\lambda=0.7}$, $N=4$	22.90	13.60	96.30	0.70	0.57
<i>B-scale, $\sim 16 \times$ compression</i>					
DyDiT $_{\lambda=0.7}$, $P=4$, isoflop	9.04	36.64	42.65	0.53	0.55
DC-DiT+ DyDiT $_{\lambda=0.7}$, $N=16$	9.08	30.12	59.72	0.56	0.51

each other. To validate this compatibility, we combine DC-DiT with DyDiT. Concretely, we modify the DiT blocks in DC-DiT by introducing gating parameters that enable the dynamic execution mechanism proposed in DyDiT. Starting from a trained DC-DiT checkpoint, the model is further trained to reduce FLOPs by 30% ($\lambda = 0.7$) for 24 epochs (120,000 steps) using a global batch size of 256 and a learning rate of 2×10^{-5} . The results are presented in Table 4. As shown, integrating DyDiT reduces FLOPs by 30% while maintaining comparable generation quality.

5 Conclusion

We introduce the Dynamic Chunking Diffusion Transformer that replaces fixed patchification with a learned, data-dependent chunking mechanism trained end-to-end with the diffusion objective. Without any explicit supervision, the mechanism discovers spatially meaningful segmentations, compressing uniform regions into fewer tokens and detail-rich regions into more tokens, and a timestep-adaptive compression schedule that allocates fewer tokens to noisy stages and more as fine details emerge. On class-conditional ImageNet 256×256 , DC-DiT consistently outperforms both parameter-matched and FLOP-matched DiT baselines across compression ratios from $4 \times$ to $16 \times$ and model scales from 138M to 690M parameters. Furthermore, we demonstrated upcycling an existing DiT checkpoint to use the dynamic chunking mechanism, and showed that our method is composable with other dynamic computation methods. We expect the principle to extend to higher resolutions and text-conditioned generation. In particular, we aim to extend our work to improve adaptive compute allocation in direct pixel-space diffusion, video generation and 3D world models.

References

[1] William Peebles and Saining Xie. Scalable diffusion models with transformers, 2023. URL <https://arxiv.org/abs/2212.09748>.

[2] Chunting Zhou, Luke Zettlemoyer, Jason Weston, Mike Lewis, Artidoro Pagnoni, Ari Holtzman, Margaret Li, Pedro Rodriguez, Lili Yu, Benjamin Muller, Gargi Ghosh, Srinivasan Iyer, Ram Pasunuru, and John Nguyen. Byte latent transformer: Patches scale better than tokens, 2024. URL <https://arxiv.org/abs/2412.09871>.

[3] Alisa Liu, Noah A. Smith, Jonathan Hayase, Yejin Choi, Sewoong Oh, and Valentin Hofmann. Superbpe: Space travel for language models, 2025. URL <https://arxiv.org/abs/2503.13423>.

[4] Sukjun Hwang, Brandon Wang, and Albert Gu. Dynamic chunking for end-to-end hierarchical sequence modeling. *arXiv preprint arXiv:2507.07955*, 2025.

[5] Xingwei Qu, Shaowen Wang, Zihao Huang, Kai Hua, Fan Yin, Rui-Jie Zhu, Jundong Zhou, Qiyang Min, Zihao Wang, Yizhi Li, Tianyu Zhang, He Xing, Zheng Zhang, Yuxuan Song, Tianyu Zheng, Zhiyuan Zeng, Chenghua Lin, Ge Zhang, and Wenhao Huang. Dynamic large concept models: Latent reasoning in an adaptive semantic space, 2026. URL <https://arxiv.org/abs/2512.24617>.

[6] Fan Wang, Yibing Song, Yang You, Jiasheng Tang, Gao Huang, Yizeng Han, Kai Wang, and Wangbo Zhao. Dynamic diffusion transformer, 2024. URL <https://arxiv.org/abs/2410.03456>.

- [7] Weinan Jia, Mengqi Huang, Nan Chen, Lei Zhang, and Zhendong Mao. D²it: Dynamic diffusion transformer for accurate image generation, 2025. URL <https://arxiv.org/abs/2504.09454>.
- [8] Zhe Lin, Wei Zhou, Yingyan Celine Lin, Yan Kang, Yuqian Zhou, Lingzhi Zhang, Zhenbang Du, Haoran You, Eli Shechtman, Yotam Nitzan, Connelly Barnes, Xiaoyang Liu, and Sohrab Amirghodsi. Layer- and timestep-adaptive differentiable token compression ratios for efficient diffusion transformers, 2024. URL <https://arxiv.org/abs/2412.16822>.
- [9] Yi Yang, Jiasheng Tang, Pichao Wang, and Shuning Chang. Flexdit: Dynamic token density control for diffusion transformer, 2024. URL <https://arxiv.org/abs/2412.06028>.
- [10] Jie Zhou, Xintao Wang, Wenliang Zhao, Pengfei Wan, Di Zhang, Mingwu Zheng, Kun Gai, Wenzhao Zheng, Jiwen Lu, Minglei Shi, Xin Tao, Haotian Yang, and Ziyang Yuan. Diffmoe: Dynamic token selection for scalable diffusion transformers, 2025. URL <https://arxiv.org/abs/2503.14487>.
- [11] Haoyu Wu, Jingyi Xu, Hieu Le, and Dimitris Samaras. Importance-based token merging for efficient image and video generation, 2025. URL <https://arxiv.org/abs/2411.16720>.
- [12] Alan Yuille, Liang-Chieh Chen, Qihang Yu, Sucheng Ren, and Ju He. Grouping first, attending smartly: Training-free acceleration for diffusion transformers, 2025. URL <https://arxiv.org/abs/2505.14687>.
- [13] Jie Zhou, Yongming Rao, Wenliang Zhao, Jiwen Lu, Cho-Jui Hsieh, and Benlin Liu. Dynamicvit: Efficient vision transformers with dynamic token sparsification, 2021. URL <https://arxiv.org/abs/2106.02034>.
- [14] Rohan Choudhury, JungEun Kim, Jinhyung Park, Eunho Yang, László A. Jeni, and Kris M. Kitani. Accelerating vision transformers with adaptive patch sizes, 2025. URL <https://arxiv.org/abs/2510.18091>.
- [15] Shivam Duggal, Phillip Isola, Antonio Torralba, and William T. Freeman. Adaptive length image tokenization via recurrent allocation, 2024. URL <https://arxiv.org/abs/2411.02393>.
- [16] Wilson Yan, Matei Zaharia, Volodymyr Mnih, Pieter Abbeel, Aleksandra Faust, and Hao Liu. Elastictok: Adaptive tokenization for image and video. *ArXiv*, abs/2410.08368, 2024. URL <https://arxiv.org/abs/2410.08368>.
- [17] Lingjun Mao, Rodolfo Corona, Xin Liang, Wenhao Yan, and Zineng Tang. Images are worth variable length of representations, 2025. URL <https://arxiv.org/abs/2506.03643>.
- [18] Yoshua Bengio, Nicholas Léonard, and Aaron Courville. Estimating or propagating gradients through stochastic neurons for conditional computation. *arXiv preprint arXiv:1308.3432*, 2013.
- [19] Robin Rombach, Andreas Blattmann, Dominik Lorenz, Patrick Esser, and Björn Ommer. High-resolution image synthesis with latent diffusion models. In *Proceedings of the IEEE/CVF Conference on Computer Vision and Pattern Recognition (CVPR)*, pages 10684–10695, June 2022.
- [20] William Fedus, Barret Zoph, and Noam Shazeer. Switch transformers: Scaling to trillion parameter models with simple and efficient sparsity. *Journal of Machine Learning Research*, 23(120):1–39, 2022.
- [21] Keshigeyan Chandrasegaran, Stefano Poli, Albert Gu, Tri Dao, and Michael S. Bernstein. Exploring diffusion transformer designs via grafting, 2025. URL <https://arxiv.org/abs/2506.05340>.